International Journal of Solids and Structures 46 (2009) 1890–1900

Contents lists available at ScienceDirect

International Journal of Solids and Structures

journal homepage: www.elsevier.com/locate/ijsolstr

Buckling of an orthotropic graded coating with an embedded crack bonded to a homogeneous substrate

W. Aloulou [a], B. Yildirim [b], S. El-Borgi [a,*], A. Zghal [c]

[a] Applied Mechanics and Systems Research Laboratory, Tunisia Polytechnic School, B.P. 743, La Marsa 2078, Tunisia
[b] Department of Mechanical Engineering, Hacettepe University, Ankara 06800, Turkey
[c] Laboratoire de Mécanique des Solides, des Structures et de Développement Technologique, Ecole Supérieure des Sciences et Techniques de Tunis, 5 Avenue Taha Houssine, Tunis 1008, Tunisia

ARTICLE INFO

Article history:
Received 20 July 2008
Received in revised form 1 December 2008
Available online 14 January 2009

Keywords:
Orthotropic graded coating
Buckling
Instability load
Nonlinear continuum theory
Perturbation technique
Singular integral equations
Finite element method

ABSTRACT

To simulate buckling of nonuniform coatings, we consider the problem of an embedded crack in a graded orthotropic coating bonded to a homogeneous substrate subjected to a compressive loading. The coating is graded in the thickness direction and the material gradient is orthogonal to the crack direction which is parallel with the free surface. The elastic properties of the material are assumed to vary continuously along the thickness direction. The principal directions of orthotropy are parallel and perpendicular to the crack orientation. The loading consists of a uniform compressive strain applied away from the crack region. The graded coating is modeled as a nonhomogeneous medium with an orthotropic stress–strain law. Using a nonlinear continuum theory and a suitable perturbation technique, the plane strain problem is reduced to an eigenvalue problem describing the onset of buckling. Using integral transforms, the resulting plane elasticity equations are converted analytically into singular integral equations which are solved numerically to yield the critical buckling strain. The Finite Element Method was additionally used to model the crack problem. The main objective of the paper is to study the influence of material nonhomogeneity on the buckling resistance of the graded layer for various crack positions, coating thicknesses and different orthotropic FGMs.

1. Introduction

In high-temperature applications the potential of using homogeneous materials appears to be limited and in recent years the new trends in material design seem to be toward coating the main load-bearing component by a heat-resistive layer, generally ceramic. Because of the relatively high mismatch in thermal expansion coefficients, the resulting bonded structure is generally subjected to relatively high residual and thermal stresses. As a result, the composite medium becomes vulnerable to cracking, debonding and spallation (Erdogan, 1995).

The materials research community has recently been exploring the possibility of using new concepts in coating design, such as Functionally Graded Materials (FGMs), as an alternative to the conventional homogeneous coatings. These can be at least two-phase inhomogeneous particulate composites synthesized in such a way that the volume fractions of the constituent materials, such as ceramic and metal, vary continuously along a spatial direction to give a predetermined composition profile resulting in a relatively smooth variation of the mechanical properties. FGMs appear to promise attractive applications in a wide variety of thermal shielding problems, such as high temperature chambers, furnace liners, turbines, micro-electronics and space structures, as well as in various wear coating problems, such as gears and cams (Holt et al., 1992). It was shown that by replacing the homogeneous ceramic coating with a FGM layer, the residual and thermal stresses would be reduced, the stress distribution would be smoother (Lee and Erdogan, 1995) and the bonding strength along the coating/substrate interface would be increased (Kurihara et al., 1990).

In designing components involving FGMs, an important problem is fracture and in particular spallation fracture. This type of failure mode is associated with the buckling instability of the cracked layer under thermally or mechanically induced compressive stress state. The buckling problem as well as the post-buckling behavior of graded coatings has been studied by a limited number of researchers using different theories under thermal and mechanical loading (Bao and Cai, 1997; Pindera et al., 2002; Shen, 2003; Ma and Wang, 2003, 2004; Liew et al., 2003; Lanhe, 2004). Chiu and Erdogan (2003) studied the buckling and post-buckling problem for the case of an interface crack between a graded coating and a semi-infinite homogeneous substrate subjected to a uniform compressive strain. The buckling problem was solved analytically using a continuum model and the post-buckling problem was

* Corresponding author. Tel.: +216 98 593 005; fax: +216 71 748 843.
E-mail address: sami.elborgi@gnet.tn (S. El-Borgi).

0020-7683/$ - see front matter © 2009 Elsevier Ltd. All rights reserved.
doi:10.1016/j.ijsolstr.2009.01.001

solved using a geometrically nonlinear finite element procedure. The same geometry was considered by El-Borgi et al. who performed a first-order analysis to compute the stress intensity factors under the effect of thermo-mechanical loading (El-Borgi et al., 2003, 2006a) and under frictional Hertzian contact loading (El-Borgi et al., 2004). El-Borgi et al. (2006b) performed a second-order analysis to study the buckling problem.

In all the above studies, the graded material considered is assumed to be isotropic. However, because of the nature of the processing techniques used in their manufacturing, FGMs are seldom isotropic. For example, Sampath et al. (1995) showed that graded materials processed by a Plasma Spray Technique generally have a lamellar structure where flattened splats and relatively weak splat boundaries create an oriented material with higher stiffness and weak cleavage planes parallel to the boundaries. Furthermore, Kaysser and Ilschner (1995) showed that graded materials processed by the Electron Beam Physical Vapour deposition technique may lead to a columnar structure which leads to higher stiffness in the thickness direction and weak facture planes perpendicular to the boundary. Therefore, in studying fracture mechanics of FGMs, the orthotropic character of these materials has to be taken into account. A limited number of studies in the literature dealt with the fracture mechanics of orthotropic FGMs. Ozturk and Erdogan (1997) studied the mode I crack problem in an orthotropic graded infinite medium with a crack perpendicular to the material gradient using the method of singular integral equations. They later extended this problem to the case of mixed-mode crack (Ozturk and Erdogan, 1999). Guo et al. (2004) investigated the mode I crack problem in a functionally graded orthotropic strip under static loading for internal crack and edge crack perpendicular to the boundaries. Guo et al. (2005) computed dynamic stress intensity factors for orthotropic FGM layers using the method of singular integral equations. Gu and Asaro (1997) performed theoretical studies to evaluate mixed-mode stress intensity factors (SIFs) and phase angles for a graded orthotropic four point bend specimen. Chen et al. (2002) studied the dynamic crack problem of a functionally graded orthotropic strip for a transient internal crack. Feng et al. (2003) considered the mode III crack problem in an orthotropic functionally graded strip. Other studies adopted finite element methodologies for fracture analysis of orthotropic FGMs, which include crack closure method (Kim and Paulino, 2002), mixed-mode J-integral (Kim and Paulino, 2003a), interaction integral (Kim and Paulino, 2003b), continuum shape sensitivity method (Rao and Rahman, 2005) and equivalent domain integral (Dag, 2006). Dag et al. (2004, 2007) and Chen (2005) used the singular integral equation method and computational techniques for the evaluation of mixed-mode stress intensity factors in orthotropic FGMs.

In this paper, we consider the plane strain buckling problem of an orthotropic graded coating bonded to a semi-infinite homogeneous medium with a crack embedded in the FGM layer and parallel to the free surface. The FGM medium is considered as a nonhomogeneous orthotropic material with a material gradient varying exponentially along the coating thickness. The principal directions of orthotropy are parallel and perpendicular to the crack orientation. The composite medium is subjected to a uniform compressive strain applied away from the crack region. Under in-plane loading, the linear elastic small deformation theory gives only a trivial solution and does not produce instability regardless of the relative dimensions and the load amplitude. Therefore, using a nonlinear continuum theory and a suitable perturbation technique, the problem is solved analytically using the method of singular integral equations as well as numerically using the finite element method resulting in an eigenvalue problem in which the instability load is evaluated numerically. The advantage of this dual approach methodology is that it permits a direct comparison between analytical and numerical results leading to the development of a reliable numerical predictive capability for this type of problems. This study is an extension of our previous work (El-Borgi et al., 2006b) in which the graded layer is modelled as isotropic instead of orthotropic.

2. Problem description and analytical formulation

As shown in Fig. 1, the problem under consideration consists of an infinitely long graded coating of thickness $h = h_1 + h_2$, bonded to a homogeneous semi-infinite medium. The graded coating contains an embedded crack of length $2a$ along the x-axis and is located at a distance h_1 from the interface and at a depth h_2 from the top surface of the coating. The composite medium is subjected to a uniform compressive strain applied away from the crack region. The graded material is assumed to be nonhomogeneous and orthotropic with a material gradient oriented along the y-direction. For the graded coating, the Poisson's ratio v is assumed to be constant because the effect of its variation on the crack-tip stress intensity factors was shown to be negligible (Delale and Erdogan, 1983; Erdogan and Wu, 1996) and is equal to the same value as that of the homogeneous substrate. The elastic stiffness constants c_{11}, c_{22}, c_{12}, c_{66} and μ_1 of the orthotropic FGM layer depend on the y-coordinate only and are assumed to be proportional with an exponential type of variation as follows (Chen et al., 2002):

$$c_{11} = c_{110}e^{\beta y}, \quad c_{22} = c_{220}e^{\beta y}, \tag{1a, b}$$

$$c_{12} = c_{120}e^{\beta y}, \quad \mu_1 = c_{66} = c_{660}e^{\beta y}, \tag{1c, d}$$

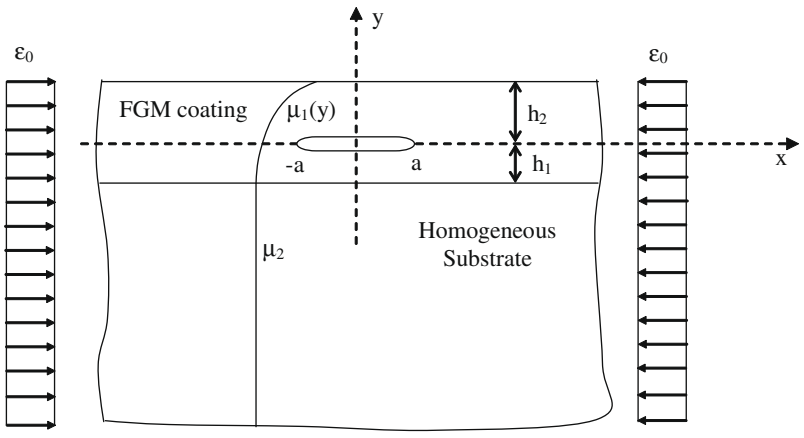

Fig. 1. Geometry and loading of the crack problem.

where c_{110}, c_{220}, c_{120}, c_{660} are the values of the material properties of the orthotropic strip along the axis $y = 0$ and β is the nonhomogeneity parameter controlling their variation in the FGM coating.

For the isotropic homogeneous substrate, the shear modulus μ_2 is a constant and is equal to the value of the FGM coating shear modulus at the interface thereby ensuring the continuity of the interface, as given below,

$$\mu_2 = c_{660}\exp(-\beta h_1). \tag{2}$$

It can be easily shown that the continuity of the mechanical properties between the two media can be imposed only in the shear modulus. It can be shown that attempting to impose the continuity of the others properties leads to a violation of the orthotropic model of the coating.

The basic equations of the plane problem in both domains are the equilibrium equations with body forces neglected, the strain–displacement relationships and the linear elastic stress–strain law. The equilibrium equations based on finite deformation theory of elasticity can be expressed as follows (Bazant and Cedolin, 2003):

$$\sigma_{ij,j} + (\sigma_{ik}u_{i,k})_{,j} = 0, \quad (i,j,k = x,y), \tag{3}$$

where u_i and σ_{ij} are, respectively, the components of the displacement and the second Piola–Kirchhoff stress.

Based on finite deformation theory of elasticity, the Green–Lagrange strain–displacement relations are given by (Bazant and Cedolin, 2003):

$$\varepsilon_{ij} = \frac{1}{2}(u_{i,j} + u_{j,i} + u_{k,i}u_{k,j}), \quad (i,j,k = x,y), \tag{4}$$

where ε_{ij} are the components of the Green–Lagrange strain tensor and the comma indicates a differentiation.

The linear elastic stress–strain law using small deformation theory of elasticity for an orthotropic material is given by

$$\sigma_{xx} = c_{11}\varepsilon_{xx} + c_{12}\varepsilon_{yy}, \tag{5a}$$
$$\sigma_{yy} = c_{12}\varepsilon_{xx} + c_{22}\varepsilon_{yy}, \tag{5b}$$
$$\sigma_{xy} = 2c_{66}\varepsilon_{xy}. \tag{5c}$$

For the FGM layer, material properties have the following expressions, for generalized plane stress conditions

$$c_{11} = \frac{E_1^2}{E_1 - E_2\nu_{12}^2}, \quad c_{22} = \frac{E_1E_2}{E_1 - E_2\nu_{12}^2},$$
$$c_{12} = \frac{E_1E_2\nu_{12}}{E_1 - E_2\nu_{12}^2}, \quad c_{66} = \mu_1, \tag{6a-d}$$

and for plane strain conditions

$$c_{11} = \frac{E_1^2(E_2 - E_3\nu_{23}^2)}{E_1(E_2 - E_3\nu_{23}^2) - E_2(E_2\nu_{12}^2 + E_3\nu_{13}(\nu_{13} + 2\nu_{12}\nu_{23}))}, \tag{7a}$$
$$c_{22} = \frac{E_2^2(E_1 - E_3\nu_{13}^2)}{E_1(E_2 - E_3\nu_{23}^2) - E_2(E_2\nu_{12}^2 + E_3\nu_{13}(\nu_{13} + 2\nu_{12}\nu_{23}))}, \tag{7b}$$
$$c_{12} = \frac{E_1E_2(E_2\nu_{12} + E_3\nu_{13}\nu_{23})}{E_1(E_2 - E_3\nu_{23}^2) - E_2(E_2\nu_{12}^2 + E_3\nu_{13}(\nu_{13} + 2\nu_{12}\nu_{23}))}, \tag{7c}$$
$$c_{66} = \mu_1, \tag{7d}$$

where E_1, E_2, E_3 are the elastic moduli in the FGM along x, y and z axes, respectively, and ν_{12}, ν_{13} and ν_{23} are the Poisson's ratios in planes xy, xz and yz, respectively.

For the homogeneous isotropic substrate, two elastic constants μ_2 and κ, namely the shear modulus and the Kolosov constant, are required to model the material stress–strain law. Instead of using μ_2 and κ, one can use four dependant parameters c_{11}, c_{22}, c_{12} and c_{66} which can be written in terms of μ_2 and κ as follows:

$$c_{11} = \mu_2\frac{1+\kappa}{\kappa-1}, \quad c_{22} = \mu_2\frac{1+\kappa}{\kappa-1}, \quad c_{12} = \mu_2\frac{3-\kappa}{\kappa-1}, \quad c_{66} = \mu_2, \tag{8a-d}$$

where $\kappa = 3 - 4\nu$ for plane strain and $\kappa = \frac{3-\nu}{1+\nu}$ for generalized plane stress in which ν is the Poisson's ratio.

A set of linearized governing equations for the buckling analysis may be obtained using the adjacent equilibrium concept which means taking a small deviation from the critical equilibrium configuration (Bazant and Cedolin, 2003). The equilibrium state is assumed to exist at a bifurcation point denoted by (0). Therefore, the displacements, stresses and deformations for a configuration adjacent to the critical state can be expressed, respectively, by

$$u_i = u_i^{(0)} + u_i^*, \quad \sigma_{ij} = \sigma_{ij}^{(0)} + \sigma_{ij}^*, \quad \varepsilon_{ij} = \varepsilon_{ij}^{(0)} + \varepsilon_{ij}^*, \tag{9a-c}$$

where the quantity with the asterisk indicates a small deviation from the critical state.

Substituting (9) into Eqs. (3) and (4) yields

$$\sigma_{ij,j}^{(0)} + (\sigma_{jk}^{(0)}u_{i,k}^{(0)})_{,j} + \sigma_{ij,j}^* + (\sigma_{jk}^{(0)}u_{i,k}^*)_{,j} + (\sigma_{jk}^*u_{i,k}^{(0)})_{,j} + (\sigma_{jk}^*u_{i,k}^*)_{,j} = 0, \tag{10}$$

$$\varepsilon_{ij}^* + \varepsilon_{ij}^{(0)} = \frac{1}{2}(u_{i,j}^{(0)} + u_{i,j}^* + u_{j,i}^{(0)} + u_{j,i}^* + u_{k,i}^{(0)}u_{k,j}^{(0)} + u_{k,i}^{(0)}u_{k,j}^* + u_{k,i}^*u_{k,j}^{(0)} + u_{k,i}^*u_{k,j}^*). \tag{11}$$

Using the equilibrium of the original configuration, neglecting the higher order terms, $(\sigma_{jk}^*u_{i,k}^*)_{,j}$ for example, and assuming that the derivatives of the displacements for the original configuration are very small ($u_{i,k}^{(0)} \ll 1$), the above equations are reduced to

$$\sigma_{ij,j}^* + (\sigma_{jk}^{(0)}u_{i,k}^*)_{,j} = 0, \quad (i,j,k = x,y), \tag{12}$$

$$\varepsilon_{ij}^* = \frac{1}{2}(u_{i,j}^* + u_{j,i}^*), \quad (i,j = x,y), \tag{13}$$

where $\sigma_{jk}^{(0)}$ are the components of the stress tensor at the boundary of the original equilibrium configuration.

To determine these components, the boundary conditions from the original equilibrium configuration are first written as follows:

$$\varepsilon_{xx}^{(0)} = -\varepsilon_0, \quad \sigma_{yy}^{(0)} = 0, \quad \sigma_{xy}^{(0)} = 0. \tag{14a-c}$$

Substituting Eqs. (14a) and (14b) into (5) gives the last component $\sigma_{xx}^{(0)}$

$$\sigma_{xx}^{(0)} = \left(\frac{c_{12}^2}{c_{22}} - c_{11}\right)\varepsilon_0. \tag{15}$$

Substituting (14b,c) and (15) into the equilibrium equations of adjacent equilibrium configuration (12) yields

$$\frac{\partial\sigma_{xx}^*}{\partial x} + \frac{\partial\sigma_{xy}^*}{\partial y} + \left(\left(\frac{c_{12}^2}{c_{22}} - c_{11}\right)\varepsilon_0\right)\frac{\partial^2u^*}{\partial x^2} = 0, \tag{16a}$$
$$\frac{\partial\sigma_{xy}^*}{\partial x} + \frac{\partial\sigma_{yy}^*}{\partial y} + \left(\left(\frac{c_{12}^2}{c_{22}} - c_{11}\right)\varepsilon_0\right)\frac{\partial^2v^*}{\partial x^2} = 0, \tag{16b}$$

where u_x^* and u_y^* were replaced in the above equations by u^* and v^*.

It is important to note that if the small deformation theory is used instead of the finite deformation theory, then the terms containing ε_0 will not appear in the above equations. In fact, these terms are present because of the inclusion of the nonlinear terms appearing in both Eqs. (3) and (4).

From the stress–strain law (5), the $(\sigma_{ij}^* - \varepsilon_{ij}^*)$ relations may be expressed as follows:

$$\sigma_{xx}^* = c_{11}\varepsilon_{xx}^* + c_{12}\varepsilon_{yy}^*, \tag{17a}$$
$$\sigma_{yy}^* = c_{12}\varepsilon_{xx}^* + c_{22}\varepsilon_{yy}^*, \tag{17b}$$
$$\sigma_{xy}^* = 2c_{66}\varepsilon_{xy}^*. \tag{17c}$$

Substituting (1a–d) and (13) into (17) and the resulting expressions into (16), the following governing equations for the buckling problem can be obtained:

$$c_{110}\frac{\partial^2 u^*}{\partial x^2}+c_{660}\frac{\partial^2 u^*}{\partial y^2}+(c_{120}+c_{660})\frac{\partial^2 v^*}{\partial x\partial y}+\beta c_{660}\frac{\partial u^*}{\partial y}+\beta c_{660}\frac{\partial v^*}{\partial x}+\left(\frac{c_{120}^2}{c_{220}}-c_{110}\right)\varepsilon_0\frac{\partial^2 u^*}{\partial x^2}=0,\quad -h_1<y\leqslant h_2, \tag{18a}$$

$$c_{660}\frac{\partial^2 v^*}{\partial x^2}+c_{220}\frac{\partial^2 v^*}{\partial y^2}+(c_{120}+c_{660})\frac{\partial^2 u^*}{\partial x\partial y}+\beta c_{120}\frac{\partial u^*}{\partial x}+\beta c_{220}\frac{\partial v^*}{\partial y}+\left(\frac{c_{120}^2}{c_{220}}-c_{110}\right)\varepsilon_0\frac{\partial^2 u^*}{\partial x^2}=0,\quad -h_1<y\leqslant h_2, \tag{18b}$$

$$(\kappa+1)\frac{\partial^2 u^*}{\partial x^2}+(\kappa-1)\frac{\partial^2 u^*}{\partial y^2}+2\frac{\partial^2 v^*}{\partial x\partial y}-8\frac{(\kappa-1)}{(\kappa+1)}\varepsilon_0\frac{\partial^2 u^*}{\partial x^2}=0,\quad y\leqslant -h_1, \tag{18c}$$

$$(\kappa-1)\frac{\partial^2 v^*}{\partial x^2}+(\kappa+1)\frac{\partial^2 v^*}{\partial y^2}+2\frac{\partial^2 u^*}{\partial x\partial y}-8\frac{(\kappa-1)}{(\kappa+1)}\varepsilon_0\frac{\partial^2 u^*}{\partial x^2}=0,\quad y\leqslant -h_1. \tag{18d}$$

For simplicity in what follows, the asterisk appearing with the quantities is omitted. The above governing equations are subject to the following boundary conditions:

$$\sigma_{xy}(x,y)=\sigma_{yy}(x,y)=0,\quad y\to-\infty,|x|<+\infty, \tag{19a,b}$$

$$\sigma_{xy}(x,h_2)=\sigma_{yy}(x,h_2)=0,\quad |x|<+\infty, \tag{20a,b}$$

$$\sigma_{xy}(x,0^+)=\sigma_{xy}(x,0^-),\quad \sigma_{yy}(x,0^+)=\sigma_{yy}(x,0^-),\quad |x|>a, \tag{21a,b}$$

$$u(x,0^+)=u(x,0^-),\quad v(x,0^+)=v(x,0^-),\quad |x|>a, \tag{22a,b}$$

$$\sigma_{xy}(x,-h_1^+)=\sigma_{xy}(x,-h_1^-),\quad \sigma_{yy}(x,-h_1^+)=\sigma_{yy}(x,-h_1^-),\quad |x|<+\infty, \tag{23a,b}$$

$$u(x,-h_1^+)=u(x,-h_1^-),\quad v(x,-h_1^+)=v(x,-h_1^-),\quad |x|<+\infty, \tag{24a,b}$$

$$\sigma_{xy}(x,0^+)=\sigma_{xy}(x,0^-)=0,\quad |x|\leqslant a, \tag{25a,b}$$

$$\sigma_{yy}(x,0^+)=\sigma_{yy}(x,0^-)=0,\quad |x|\leqslant a. \tag{26a,b}$$

Eqs. (19a,b) represent the regularity conditions at infinity $y\to-\infty$ meaning vanishing stresses at $y\to-\infty$. Eqs. (20a,b) indicate that the top surface of the graded coating is free of tractions. Eqs. (21a,b) and (22a,b) describe, respectively, the continuity of stresses and displacements along the crack plane and outside the crack. Eqs. (23a,b) and (24a,b) describe, respectively, the continuity of stresses and displacements at the interface between the two materials. Finally, Eqs (25a,b) and (26a,b) indicate that no tractions are applied on the crack surfaces.

The following dimensionless quantities are defined and the bar appearing in these quantities is omitted thereafter for simplicity:

$$\bar{\sigma}_{ij}=\sigma_{ij}/c_{660},\quad \bar{\beta}=\beta a, \tag{27a,b}$$

$$(\bar{x},\bar{y})=(x,y)/a,\quad (\bar{u},\bar{v})=(u,v)/a, \tag{27c,d}$$

$$\bar{c}_{110}=c_{110}/c_{660},\quad \bar{c}_{220}=c_{220}/c_{660},\quad \bar{c}_{120}=c_{120}/c_{660}. \tag{27e,f}$$

3. Singular integral equations

The plane elasticity equations (18a–d) are solved using standard Fourier transforms to yield the displacement field in the graded coating and in the homogeneous substrate which is expressed as follows:

$$u(x,y)=\int_{-\infty}^{+\infty}\sum_{k=1}^{4}C_k(\lambda)e^{m_k y}e^{-ix\lambda}d\lambda,\quad 0<y\leqslant h_2, \tag{28a}$$

$$v(x,y)=\int_{-\infty}^{+\infty}\sum_{k=1}^{4}C_k s_k(\lambda)e^{m_k y}e^{-ix\lambda}d\lambda,\quad 0<y\leqslant h_2, \tag{28b}$$

$$u(x,y)=\int_{-\infty}^{+\infty}\sum_{k=1}^{4}C_{k+4}(\lambda)e^{m_k y}e^{-ix\lambda}d\lambda,\quad -h_1<y\leqslant 0, \tag{28c}$$

$$v(x,y)=\int_{-\infty}^{+\infty}\sum_{k=1}^{4}C_{k+4}s_k(\lambda)e^{m_k y}e^{-ix\lambda}d\lambda,\quad -h_1<y\leqslant 0, \tag{28d}$$

$$u(x,y)=\int_{-\infty}^{+\infty}\sum_{k=1}^{4}C_{k+8}(\lambda)e^{n_k y}e^{-ix\lambda}d\lambda,\quad y\leqslant -h_1, \tag{28e}$$

$$v(x,y)=\int_{-\infty}^{+\infty}\sum_{k=1}^{4}C_{k+8}s_{k+4}(\lambda)e^{n_k y}e^{-ix\lambda}d\lambda,\quad y\leqslant -h_1. \tag{28f}$$

In the above equations, the unknown functions $C_{11}(\lambda)$ and $C_{12}(\lambda)$ are both zero after applying the regularity conditions (19a,b), while the remaining unknowns $C_k(\lambda)$ $(k=1,\ldots,10)$ are unknown functions determined from the boundary conditions (20)–(24). $m_k(\lambda)$ $(k=1,\ldots,4)$ are the roots of the characteristic polynomial associated with the plane elasticity equations for the graded coating (18a,b) and $n_k(\lambda)$ $(k=1,\ldots,4)$ are the roots of the characteristic polynomial associated with the plane elasticity equations for the homogeneous substrate (18c,d) which are all expressed as follows:

$$m_1=\left(-\frac{\beta}{2}-\sqrt{\frac{\beta^2}{4}+2\kappa_0\lambda^2+4\lambda\sqrt{(\kappa_0^2-\delta)\lambda^2-\beta^2 v_0}}\right), \tag{29a}$$

$$m_2=\left(-\frac{\beta}{2}-\sqrt{\frac{\beta^2}{4}+2\kappa_0\lambda^2-4\lambda\sqrt{(\kappa_0^2-\delta)\lambda^2-\beta^2 v_0}}\right), \tag{29b}$$

$$m_3=\left(-\frac{\beta}{2}+\sqrt{\frac{\beta^2}{4}+2\kappa_0\lambda^2+4\lambda\sqrt{(\kappa_0^2-\delta)\lambda^2-\beta^2 v_0}}\right), \tag{29c}$$

$$m_4=\left(-\frac{\beta}{2}+\sqrt{\frac{\beta^2}{4}+2\kappa_0\lambda^2-4\lambda\sqrt{(\kappa_0^2-\delta)\lambda^2-\beta^2 v_0}}\right), \tag{29d}$$

$$n_1=\sqrt{1-\frac{8\varepsilon_0}{(\kappa+1)}}|\lambda|,\quad n_2=\sqrt{1-\frac{8(\kappa-1)}{(\kappa+1)^2}\varepsilon_0}|\lambda|, \tag{30a,b}$$

$$n_3=-\sqrt{1-\frac{8\varepsilon_0}{(\kappa+1)}}|\lambda|,\quad n_4=-\sqrt{1-\frac{8(\kappa-1)}{(\kappa+1)^2}\varepsilon_0}|\lambda|, \tag{30c,d}$$

where κ_0, δ, v_0 and $s_k(k=1,\ldots,6)$ are, respectively, given by Eqs. (A.1)–(A.7).

We now introduce the density functions

$$\psi_1(x)=\frac{\partial}{\partial x}[u(x,0^+)-u(x,0^-)],\quad \psi_2(x)=\frac{\partial}{\partial x}[v(x,0^+)-v(x,0^-)], \tag{31a,b}$$

which satisfy the following single-valuedness conditions:

$$\int_{-1}^{+1}\psi_j(t)dt=0\quad (j=1,2),\quad \psi_j(x)=0\quad (j=1,2)\quad |x|\geqslant 1. \tag{32a,b}$$

Applying the boundary conditions (20)–(24) yields the linear system of equations given by (A.8a–j) in which the unknown functions $C_k(\lambda)$ $(k=1,\ldots,10)$ are expressed in terms of the unknown density functions ψ_1 and ψ_2.

Applying the remaining boundary conditions (25) and (26) yields the following coupled singular integral equations in which the unknowns are the density functions ψ_1 and ψ_2 and which after extracting the Cauchy singularity from the kernels take the following form:

$$\int_{-1}^{+1}\left[\left(\frac{a_0}{t-x}+k_{11}(x,t)\right)\psi_1(t)+k_{12}(x,t)\psi_2(t)\right]dt=0,\quad |x|\leqslant 1, \tag{33a}$$

$$\int_{-1}^{+1}\left[k_{21}(x,t)\psi_1(t)+\left(\frac{d_0}{t-x}+k_{22}(x,t)\right)\psi_2(t)\right]dt=0,\quad |x|\leqslant 1, \tag{33b}$$

where the known functions $k_{11}(x,t)$, $k_{12}(x,t)$, $k_{21}(x,t)$ and $k_{22}(x,t)$ are Fredholm kernels that depend on the nonhomogeneity parameterβ and whose expressions are given by (A.16), and a_0 and d_0, which are given by Eqs. (A.21) and (A.22), are the coefficients of the leading terms corresponding to the Cauchy singularity of the kernels obtained after a lengthy asymptotic analysis.

It was shown in Erdogan et al. (1973) that the solution of (33a,b) subject to the single-valuedness condition (33a) may be expressed as $\psi_i(t)=w(t)\phi_i(t)$ $(i=1,2)$. In this solution, $w(t)=1/\sqrt{1-t^2}$ is the weight function which is obtained from the nature of the singularity at the crack tips and which is associated with the Chebyshev polynomial of the first kind $T_n(t)=\cos(n\arccos(t))$. The functions $\phi_i(t)$ $(i=1,2)$ are continuous and bounded function in the interval $[-1,1]$ which may be expressed as a truncated series of Chebyshev polynomial of the first kind. Therefore, the solution of (33a,b) may be expressed as

$$\psi_1(t)=\sum_{n=1}^{N}\tilde{a}_nT_n(t)/\sqrt{1-t^2},\quad \psi_2(t)=\sum_{n=1}^{N}\tilde{b}_nT_n(t)/\sqrt{1-t^2}. \tag{34a,b}$$

Substituting (34) into (33), we obtain two linear algebraic equations for the unknowns $\tilde{a}_1,\ldots,\tilde{a}_N,\tilde{b}_1,\ldots,\tilde{b}_N$ in addition to ε_0

$$\sum\nolimits_{n=1}^{N}\tilde{a}_n[\pi U_{n-1}(x)+H_{11}^n(x)]+\sum_{n=1}^{N}\tilde{b}_n[H_{12}^n(x)]=0,\quad |x|\leqslant 1, \tag{35a}$$

$$\sum\nolimits_{n=1}^{N}\tilde{a}_n[H_{21}^n(x)]+\sum_{n=1}^{N}\tilde{b}_n[\pi U_{n-1}(x)+H_{22}^n(x)]=0,\quad |x|\leqslant 1, \tag{35b}$$

where $U_{n-1}(x)$ is the Chebyshev polynomial of the second kind and $H_{ij}^n(x)$ $(i,j=1,2)$ are given by

$$U_{n-1}(x)=\frac{\sin(n\arccos(x))}{\sqrt{1-x^2}},\quad H_{ij}^n(x)=\int_{-1}^{1}\frac{T_n(t)}{\sqrt{1-t^2}}k_{ij}(x,t)dt. \tag{36a,b}$$

Using a suitable collocation method (Erdogan and Wu, 1996), Eqs. (35a,b) are converted to the following linear algebraic system in $\tilde{a}_1,\ldots,\tilde{a}_N,\tilde{b}_1,\ldots,\tilde{b}_N$ which is nonlinear in terms of the unknown ε_0:

$$\begin{bmatrix} A_1^1(x_1) & \cdots & A_N^1(x_1) & A_1^2(x_1) & \cdots & A_N^2(x_1)\\ \vdots & \cdots & \vdots & \vdots & \cdots & \vdots\\ A_1^1(x_N) & \cdots & A_N^1(x_N) & A_1^2(x_N) & \cdots & A_N^2(x_N)\\ A_1^3(x_1) & \cdots & A_N^3(x_1) & A_1^4(x_1) & \cdots & A_N^4(x_1)\\ \vdots & \cdots & \vdots & \vdots & \cdots & \vdots\\ A_1^3(x_N) & \cdots & A_N^3(x_N) & A_1^4(x_N) & \cdots & A_N^4(x_N)\end{bmatrix}\begin{Bmatrix}\tilde{a}_1\\ \vdots\\ \tilde{a}_N\\ \tilde{b}_1\\ \vdots\\ \tilde{b}_N\end{Bmatrix}=\begin{Bmatrix}0\\ \vdots\\ 0\\ 0\\ \vdots\\ 0\end{Bmatrix}, \tag{37}$$

where the coefficients $A_i^k(x_j)$ $(i,j=1,\ldots,N;k=1,\ldots,4)$ are given by

$$A_i^k(x_j)=\pi U_{i-1}(x_j)+H_{kk}^i(x_j),\quad (i,j=1,\ldots,N;\quad k=1,4), \tag{38a}$$

$$A_i^2(x_j)=H_{12}^i(x_j),\quad A_i^3(x_j)=H_{21}^i(x_j),\quad (i,j=1,\ldots,N). \tag{38b,c}$$

The components of the matrix in (37) are nonlinear functions of ε_0. Since the right hand side of (37) is equal to zero, this equation represents, therefore, an eigenvalue problem with the eigenvalue being ε_0 and the eigenvector being $\{\tilde{a}_1\ \ldots\ \tilde{a}_N\ \tilde{b}_1\ \ldots\ \tilde{b}_N\}^T$. For non-trivial solutions of $\tilde{a}_i$ and $\tilde{b}_i$ $(i=1,\ldots,N)$, the determinant of the matrix in (37) must be zero. The determinant in (37) is a monotonically decreasing nonlinear function of ε_0 up to the first critical compressive strain $(\varepsilon_0)_{cr}$ where the determinant will vanish. Therefore, a simple iterative scheme was adopted to obtain the critical compressive strain $(\varepsilon_0)_{cr}$ corresponding to the buckling of the coating. From the nature of the eigenvalue problem, the exact values of $\{\tilde{a}_1\ \ldots\ \tilde{a}_N\ \tilde{b}_1\ \ldots\ \tilde{b}_N\}^T$ cannot be obtained unless within a multiplicative arbitrary constant.

4. Finite element formulation

In addition to the singular integral equation method, the general purpose finite element program ANSYS (2007) commercial software is used to estimate the critical eigen strains $(\varepsilon_0)_{cr}$. The buckling problem may be written as follows:

$$[K]\{\phi_i\}=\lambda_i[S]\{\phi_i\}, \tag{39}$$

where $\{\phi_i\}$ are the eigenvectors, λ_i are the eigenvalues and $[K]$ is the plane strain stiffness matrix defined over an area integration as follows:

$$[K]=\int_A[B]^T[D][B]dA, \tag{40}$$

in which the matrix $[B]$ contains derivatives of the shape functions N_i $(i=1,\ldots,6)$ for a six-node triangular element used in the analysis.

$$[B]=\begin{bmatrix}\frac{\partial N_i}{\partial x} & 0\\ 0 & \frac{\partial N_i}{\partial y}\\ \frac{\partial N_i}{\partial y} & \frac{\partial N_i}{\partial x}\end{bmatrix}, \tag{41}$$

and the matrix $[D]$ contains material properties in terms of Poisson's ratios, elastic and shear moduli, which is defined as the inverse of compliance matrix $[C]$ as

$$[D]^{-1}=[C]=\begin{bmatrix}\frac{1}{E_1} & -\frac{\nu_{12}}{E_1} & 0\\ -\frac{\nu_{21}}{E_2} & \frac{1}{E_2} & 0\\ 0 & 0 & \frac{1}{G_{12}}\end{bmatrix}. \tag{42}$$

In Eq. (39), the matrix $[S]$ is the stress stiffness matrix given by

$$[S]=\begin{bmatrix}[S_0] & 0\\ 0 & [S_0]\end{bmatrix}, \tag{43}$$

where $[S_0]$ is a 6×6 matrix given as the integral over an area

$$[S_0]=\int_A[S_g]^T[S_m][S_g]dA, \tag{44}$$

in which

$$[S_m]=\begin{bmatrix}\sigma_x & \sigma_{xy} & 0\\ \sigma_{xy} & \sigma_y & 0\\ 0 & 0 & \sigma_z\end{bmatrix}, \tag{45}$$

where σ_x, σ_{xy}, etc. are stresses based on the displacements of the previous iteration, and, $[S_g]$ is a matrix containing the derivatives of shape functions N_i $(i=1,\ldots,6)$ for a six-node triangular element used in the analysis.

$$[S_g]=\begin{bmatrix}\frac{\partial N_1}{\partial x} & \frac{\partial N_2}{\partial x} & \cdots & \frac{\partial N_6}{\partial x}\\ \frac{\partial N_1}{\partial y} & \frac{\partial N_2}{\partial y} & \cdots & \frac{\partial N_6}{\partial y}\end{bmatrix}. \tag{46}$$

Eq. (39) must be transformed to the standard eigenvalue problem which may be written as follows:

$$[A]\{\psi\} = \lambda\{\psi\}, \tag{47}$$

where $[A]$ is a symmetric matrix and the eigenvectors $\{\psi\}$ and $\{\phi_i\}$ are related by

$$\{\phi_i\} = [L]^{-T}\{\psi\}, \tag{48}$$

in which $[L]$ is a lower triangular matrix obtaining by decomposing the matrix $[S]$ in (39) into a lower and an upper triangular matrix

$$[S] = [L][L]^T. \tag{49}$$

Premultiplying both sides of Eq. (39) by the matrix $[S]^{-1}$, substituting (48) and (49) into the resulting expression and simplifying by $[L]^{-T}$ yields the equation of the standard eigenvalue problem (47), where $[A]$ is given by

$$[A] = [L]^{-1}[S][L]^{-T}. \tag{50}$$

Block Lanczos method, which is a variation of the classical Lanczos algorithm, is used for the eigenvalue extraction (ANSYS, 2007). In Block Lanczos algorithm, the Lanczos recursions are performed using a block of vectors whereas in classical Lanczos method a single vector is used. Details of Lanczos method and its application to the finite element method will not be discussed here and can be found in references (Release 11 documentation for ANSYS, 2007; Grimes et al., 1994; Rajakumar and Rogers, 1991).

Triangular PLANE2 elements, with quadratic interpolation, are used for the analysis. These elements have six nodes as one at each corner and ones in midge edges (Fig. 2). Material properties are assigned according to centroidal coordinate of each element and are constant within each element. Convergence check is carefully performed and the number of elements is determined such that increasing the number of elements does not change the significant digits of the results. This implies that element refinement is sufficient to capture the correct material property gradation and accurate results. In order to reduce modeling time, Ansys Parametric Design Language (APDL) is used. APDL is a scripting language that one can use to automate common tasks and build a model in terms of parameters. In particular, the definition of graded orthotropic material properties can only be accomplished with APDL.

In the finite element model, the crack length is chosen as 1 unit. For example for $h_2/a = 0.07$ ratio $a = 1$ and $h_2 = 0.07$ units are used. Half of the problem is modeled taking the advantage of the symmetry. The length of the model is taken as $100a$ to prevent the free surface effect on the eigen strains and to be able to simulate an infinitely long medium. The height of the substrate is taken as $50a$ to be able to simulate a semi-infinite medium. These dimensions are also determined such that the increase in any dimension has no affect on the eigen strains.

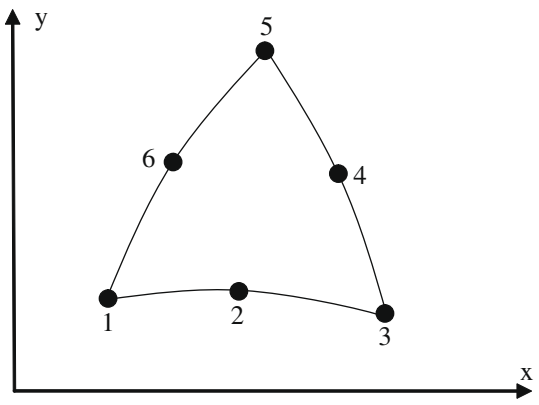

Fig. 2. PLANE2, six-node triangular element.

A typical deformed mesh of the model is shown in Fig. 3. Models have around 50,000 triangular elements depending on h_1/a, h_2/a ratios. Results obtained from ANSYS are the critical displacements at the far edge for the buckling to occur. Later these results are converted to critical strains $(\varepsilon_0)_{cr}$ simply by dividing the critical displacement by the length of the model.

5. Results and discussion

Similar formulation using singular integral equations to determine the critical buckling load for the case of isotropic graded coatings was already published by El-Borgi et al. (2006b). To verify our present formulation, we solved the problem of an isotropic nonhomogeneous coating by letting $c_{11} = \mu_1(\kappa + 1)/(\kappa - 1)$, $c_{12} = \mu_1(3 - \kappa)/(\kappa - 1)$, $c_{11} = c_{22}$ and $c_{66} = \mu_1$, where $\kappa = 3 - 4\nu$ for plain strain. The Poisson's ratio ν is taken equal to 0.3. The obtained results were in excellent agreement with those reported in our previous paper (El-Borgi et al., 2006b).

To study the effect of material orthotropy on the critical buckling load, calculations were carried out, under the assumption of plane strain conditions, for five kinds of orthotropic materials whose mechanical properties are obtained from Guo et al. (2004) and are listed in Table 1. Orthotropic material 2 has a higher stiffness value of c_{220} than orthotropic material 1. The difference between orthotropic 2 and 3 is that their reinforced directions are perpendicular to each other. Orthotropic material 4 has a higher value of c_{110} compared to material 1. Orthotropic material 5 has a higher value of c_{120} compared to material 4.

5.1. Comparison between continuum model and finite element results

A number of simulations were performed by varying βh from a compliant coating ($\beta h < 0$) to a stiff one ($\beta h > 0$) in the interval $[-3,+3]$. The results, which are presented hereafter, were obtained for different crack depth positions and constant coating thickness: $h_1/h_2 = 0/0.07$, 5/9, 1/1, and $(h_1 + h_2) = 0.07a$; and for different FGM coating thicknesses and a constant crack depth position: $h_1 = 0.025a$, $h_2 = 0.035a$, $0.045a$, $0.055a$, $0.065a$.

Fig. 4a and b shows a comparison between analytically and numerically computed buckling load $(\varepsilon_0)_{cr}$ obtained, respectively, using the singular integral equation method and the finite element method. The reported results are obtained for materials 1 and 2 and for different crack depth positions and constant coating thickness: $h_1/h_2 = 0/0.07$, 5/9, 1/1, and $(h_1 + h_2) = 0.07a$. It is clear that the numerical results are very close to the analytical ones although differences in the results might be noticed for large values of βh especially when the crack is at the interface $h_1 = 0$. However, for material 2, a small discrepancy between numerical and analytical results for the case of an interfacial crack with a relative error varying between 2% and 5%, is illustrated in Fig. 4b. An excellent agreement is obtained for materials 3, 4 and 5 but the results are not reported.

Fig. 5a and b shows a comparison between analytical and numerical results obtained for different FGM coating thicknesses and a constant crack depth position: $h_1 = 0.025a$ for materials 1 and 2. It can be noticed that the numerical results are very close to the analytical ones. Similar observations are found for materials 3, 4 and 5.

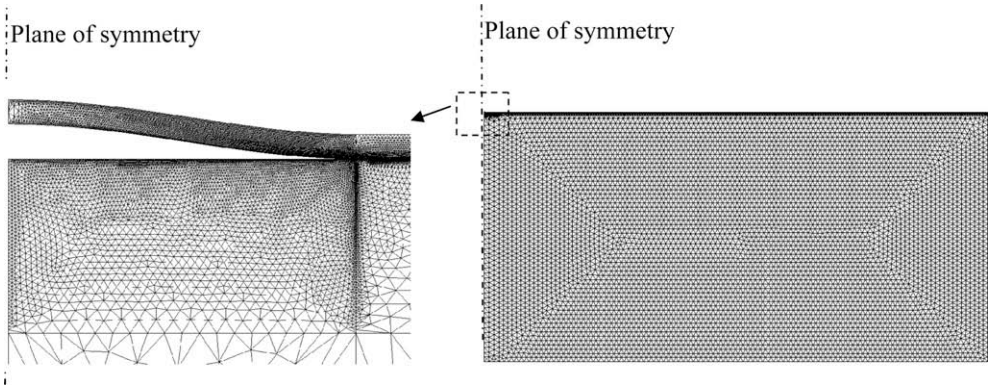

Fig. 3. Deformed finite element mesh (scale = 1) $h_1/a = 0$, $h_2/a = 0.07$.

Table 1
Mechanical properties of FGM coatings.

Material	c_{110} (N/m^2)	c_{120} (N/m^2)	c_{220} (N/m^2)	c_{660} (N/m^2)
Orthotropic 1	1.048×10^{10}	3.248×10^{9}	1.578×10^{10}	7.070×10^{9}
Orthotropic 2	1.048×10^{10}	3.248×10^{9}	4.192×10^{10}	7.070×10^{9}
Orthotropic 3	4.192×10^{10}	3.248×10^{9}	1.048×10^{10}	7.070×10^{9}
Orthotropic 4	4.192×10^{10}	3.248×10^{9}	1.578×10^{10}	7.070×10^{9}
Orthotropic 5	4.192×10^{10}	10.605×10^{9}	1.578×10^{10}	7.070×10^{9}
Isotropic	2.475×10^{10}	10.605×10^{9}	2.475×10^{10}	7.070×10^{9}

It can be concluded then that for all the cases investigated the numerical results are very close to the analytical ones which indicates the accuracy of the predictive capability of ANSYS at least for this problem.

5.2. Buckling load for different orthotropic materials

Fig. 6a and b shows the variation of the critical compressive strain $(\varepsilon_0)_{cr}$ with varying values of βh for the different orthotropic

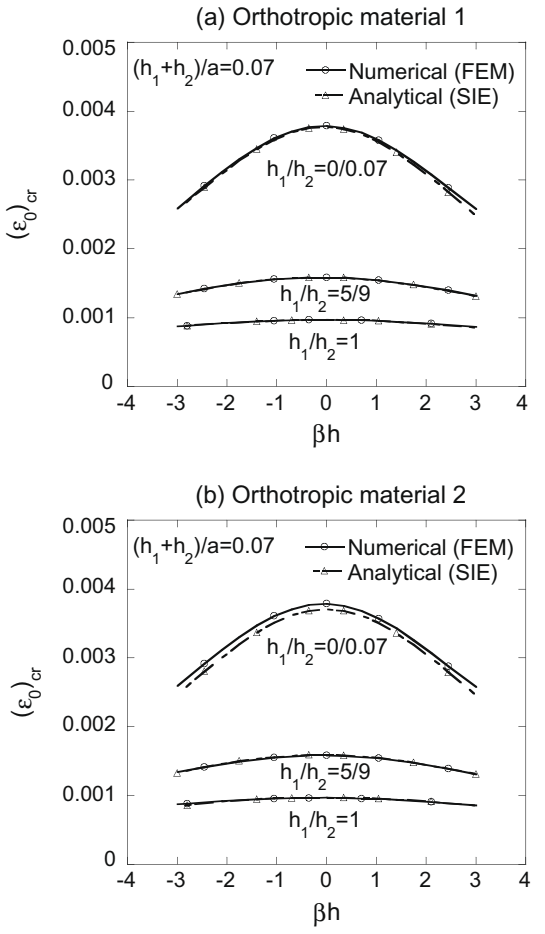

Fig. 4. (a and b) Analytical and numerical predictions of the instability strain $(\varepsilon_0)_{cr}$ for varying values of the nonhomogeneity parameter βh for different crack depth positions and constant coating thickness, $h_1/h_2 = 0/0.07$, 5/9, 1/1, $(h_1 + h_2)/a = 0.07$ for orthotropic materials 1 and 2.

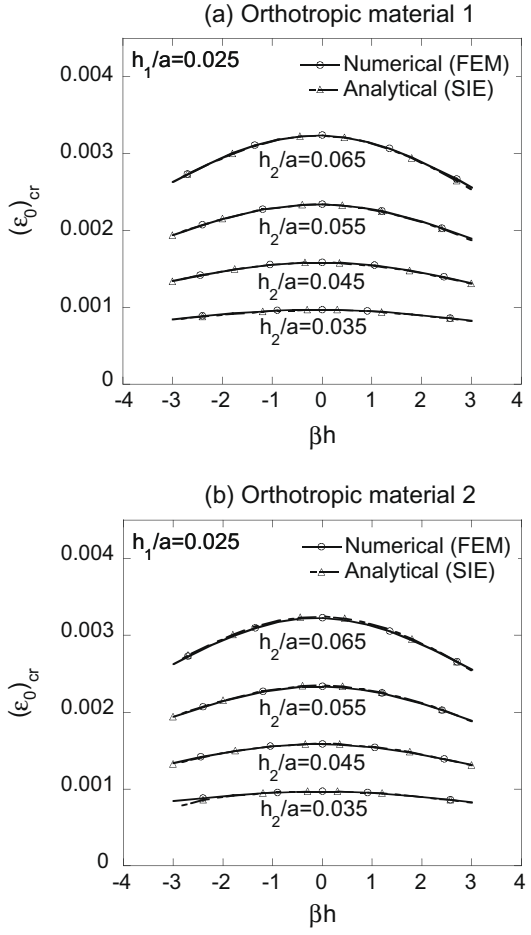

Fig. 5. (a and b) Analytical and numerical predictions of the instability strain $(\varepsilon_0)_{cr}$ for varying values of the nonhomogeneity parameter βh for a fixed crack position and different FGM coating thicknesses, $h_1/a = 0.025$, $h_2/a = 0.035$, 0.045, 0.055, 0.065 for orthotropic materials 1 and 2.

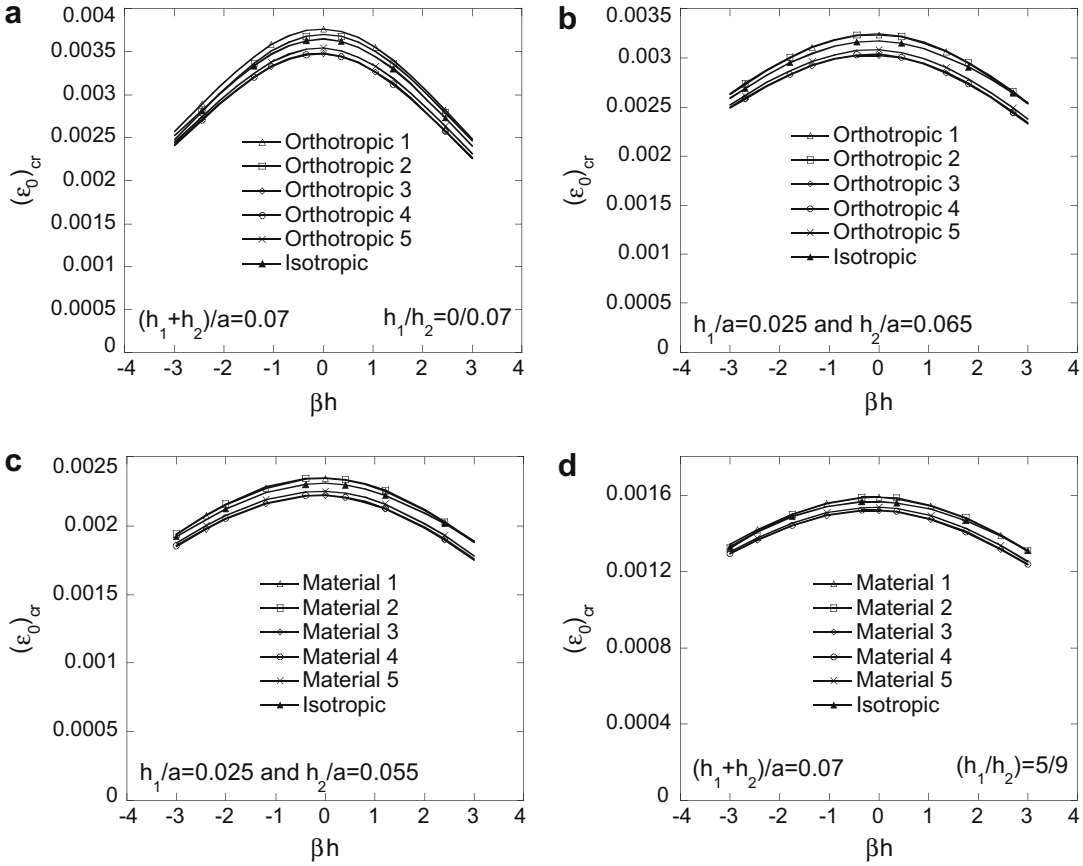

Fig. 6. Effect of the orthotropic parameters on the instability strain $(\varepsilon_0)_{cr}$ with varying values of the nonhomogeneity parameter βh (a) for an interfacial crack where $h_1/a = 0$ and $h_2/a = 0.07$; (b) for a crack in the FGM where $h_1/a = 0.025$ and $h_2/a = 0.065$; (c) for a crack in the FGM where $h_1/a = 0.025$ and $h_2/a = 0.055$; (d) for a crack in the FGM where $(h_1 + h_2)/a = 0.07$ and $h_1/h_2 = 5/9$.

and isotropic coatings for different crack locations. It is clear that when the crack gets closer to the surface of the coating, the instability load is at its smallest value and becomes insensitive to variations in the nonhomogeneity parameter βh. The critical strain reaches a maximum value for a homogeneous coating (i.e., $\beta h = 0.0001$) and it decreases for both compliant and stiff coatings.

Four cases of crack locations are presented, namely for a crack embedded in the graded coating ($h_1/a = 0.025$ and $h_2/a = 0.065$, 0.055, 0.045) and an interfacial crack ($h_1/a = 0$ and $h_2/a = 0.07$). Similar observations are found for the other crack locations. As shown in Fig. 6a–d, comparing the curves for materials 1 and 2, it is observed that they coincide for almost all the cases of crack location except for the case where the crack is at the interface. For the latter case, buckling strains for material 2 are lower than those for material 1. It can be concluded that the change of the stiffness parameter c_{220} has no effect on the buckling strain when the crack is embedded in the FGM coating. For an interfacial crack, an increase in the c_{220} parameter causes a small decrease in the buckling strains.

Comparing the curves for materials 3 and 4, it is observed that they coincide for all the cases of crack location including the case where the crack is at the interface. Materials 3 and 4 have the same value of c_{110} which is higher than that of materials 1 and 2. The change of the parameter c_{220} for materials 3 and 4 is lower than the change of the parameter c_{220} for materials 1 and 2. Therefore, it is shown that the parameter c_{220} has no effect on the buckling strain for all the cases.

Comparing the curves for materials 1 and 4, the effect of the change of the parameter c_{110} can be observed. Material 4 has larger value of c_{110}. It is clear that an increase in c_{110} causes a decrease in critical buckling strains at any crack location.

Comparing the curves for materials 4 and 5, the effect of the change of the parameter c_{120} can be observed. An increase in the c_{120} parameter yields an increase in critical buckling strains at any crack location.

Results for isotropic FGM coatings are also plotted. They are shown with filled triangles. The corresponding curves are located between the curves of the other orthotropic materials. It can be concluded that considering FGM coatings as isotropic materials is an average approximation. However, the difference in the buckling strains for isotropic and orthotropic material is very well noticed.

6. Conclusion

In this paper, we considered the plane strain buckling problem of an orthotropic graded coating bonded to a homogeneous semi-infinite medium with a crack embedded in the FGM layer and parallel to the free surface. Using a nonlinear continuum theory and a suitable perturbation technique, the problem was solved analytically using the method of singular integral equations as well as numerically using the finite element method. A detailed parametric study was conducted to investigate the effect of the material nonhomogeneity parameter on the buckling resistance of the graded layer for various crack positions, coating thicknesses and different orthotropic FGMs. It can be concluded from this study that the numerical results are very close to the analytical ones

which indicates the accuracy of the predictive capability of ANSYS at least for this problem. In addition, considering FGM coatings as isotropic materials is found to be an average approximation and the difference in the buckling strains for isotropic and orthotropic material is very well noticed.

Appendix A

Expressions of the quantities appearing in Eq. (29):

$$\kappa_0 = \frac{1}{2}\left[\frac{1}{c_{220}}(1+X_0) + (c_{110}+X_0) - \frac{(c_{120}+1)^2}{c_{220}}\right], \tag{A.1}$$

$$\delta = \frac{1}{c_{220}}(c_{110}+X_0)(1+X_0), \tag{A.2}$$

$$v_0 = \frac{c_{120}}{c_{220}}, \tag{A.3}$$

with

$$X_0 = \left(\frac{c_{120}^2}{c_{220}} - c_{110}\right)\varepsilon_0. \tag{A.4}$$

Expressions of the known functions $s_k(\lambda)$ ($k = 1,\ldots,6$) given in Eq. (28):

$$s_k = \frac{i\lambda((c_{120}+1)m_k + \beta c_{120})}{c_{220}m_k^2 + \beta c_{220}m_k - (1+X_0)\lambda^2} \quad (k = 1,\ldots,4), \tag{A.5}$$

$$s_5 = \frac{i\lambda}{n_1}, \quad s_6 = i\frac{n_2}{\lambda}. \tag{A.6-7}$$

Linear system of equations obtained after applying the boundary conditions (20)–(24):

$$\sum_{k=1}^{4} p_k C_k e^{m_k h_2} = 0, \tag{A.8a}$$

$$\sum_{k=1}^{4} q_k C_k e^{m_k h_2} = 0, \tag{A.8b}$$

$$\sum_{k=1}^{4} q_k C_k - \sum_{k=1}^{4} q_k C_{k+4} = 0, \tag{A.8c}$$

$$\sum_{k=1}^{4} p_k C_k - \sum_{k=1}^{4} p_k C_{k+4} = 0, \tag{A.8d}$$

$$\sum_{k=1}^{4} q_k C_{k+4} e^{-m_k h_1} e^{-\beta h_1} - q_5 C_9 e^{-n_1 h_1} - q_6 C_{10} e^{-n_2 h_1} = 0, \tag{A.8e}$$

$$\sum_{k=1}^{4} p_k C_{k+4} e^{-m_k h_1} e^{-\beta h_1} - p_5 C_9 e^{-n_1 h_1} - p_6 C_{10} e^{-n_2 h_1} = 0, \tag{A.8f}$$

$$\sum_{k=1}^{4} C_{k+4} e^{-m_k h_1} - C_9 e^{-n_1 h_1} - C_{10} e^{-n_2 h_1} = 0, \tag{A.8g}$$

$$\sum_{k=1}^{4} s_k C_{k+4} e^{-m_k h_1} - s_5 C_9 e^{-n_1 h_1} - s_6 C_{10} e^{-n_2 h_1} = 0, \tag{A.8h}$$

$$C_1 + C_2 + C_3 + C_4 - C_5 - C_6 - C_7 - C_8 = F_1, \tag{A.8i}$$

$$s_1 C_1 + s_2 C_2 + s_3 C_3 + s_4 C_4 - s_1 C_5 - s_2 C_6 - s_3 C_7 - s_4 C_8 = F_2, \tag{A.8j}$$

where

$$F_j(\lambda) = \frac{i}{2\pi\lambda}\int_{-1}^{+1} \psi_j(t) e^{it\lambda} dt \quad (j = 1,2), \tag{A.9}$$

and q_k, p_k ($k = 1,\ldots,6$) are functions of λ which depend also on the nonhomogeneity parameter β and their expressions are given by

$$p_k = -i\lambda c_{120} + c_{220} m_k s_k \quad (k = 1,\ldots,4), \tag{A.10}$$

$$p_5 = 2i\lambda, \quad p_6 = (i\lambda)\left[-\left(\frac{3-\kappa}{\kappa-1}\right) + \left(\frac{\kappa+1}{\kappa-1}\right)\left(\frac{n_2}{\lambda}\right)^2\right], \tag{A.11-12}$$

$$q_k = m_k - i\lambda s_k \quad (k = 1,\ldots,4), \tag{A.13}$$

$$q_5 = n_1 - i\lambda s_5, \quad q_6 = n_2 - i\lambda s_6. \tag{A.14-15}$$

Expressions of quantities appearing in (33):

$$K_{ii}(x,t) = \lim_{y\to 0^-}\int_0^{+\infty} (N_{ii}(y,\lambda)\sin\lambda(t-x))d\lambda \quad (i = 1,2) \tag{A.16a}$$

$$K_{ij}(x,t) = \lim_{y\to 0^-}\int_0^{+\infty} (M_{ij}(y,\lambda)\cos\lambda(t-x))d\lambda \quad (i,j = 1,2) \text{ and } i \neq j, \tag{A.16b}$$

where

$$N_{11}(y,\lambda) = -\frac{2}{\lambda}\left(q_1\frac{D_9^5}{D}e^{m_1 y} - q_2\frac{D_9^6}{D}e^{m_2 y} + q_3\frac{D_9^7}{D}e^{m_3 y} - q_4\frac{D_9^8}{D}e^{m_4 y}\right), \tag{A.17}$$

$$N_{22}(y,\lambda) = -\frac{2}{\lambda}\left(-p_1\frac{D_{10}^5}{D}e^{m_1 y} + p_2\frac{D_{10}^6}{D}e^{m_2 y} - p_3\frac{D_{10}^7}{D}e^{m_3 y} + p_4\frac{D_{10}^8}{D}e^{m_4 y}\right), \tag{A.18}$$

$$M_{12}(y,\lambda) = \frac{2i}{\lambda}\left(-q_1\frac{D_{10}^5}{D}e^{m_1 y} + q_2\frac{D_{10}^6}{D}e^{m_2 y} - q_3\frac{D_{10}^7}{D}e^{m_3 y} + q_4\frac{D_{10}^8}{D}e^{m_4 y}\right), \tag{A.19}$$

$$M_{21}(y,\lambda) = \frac{2i}{\lambda}\left(p_1\frac{D_9^5}{D}e^{m_1 y} - p_2\frac{D_9^6}{D}e^{m_2 y} + p_3\frac{D_9^7}{D}e^{m_3 y} - p_4\frac{D_9^8}{D}e^{m_4 y}\right), \tag{A.20}$$

where D is the determinant of the (10×10) matrix and D_i^j ($i = 9,10$ and $j = 5,\ldots,8$) are the sub-determinants determinants obtained by the elimination of the ith row and the jth column.

Expressions of a_0 and d_0 , appearing in (33):

$$a_0 = -\left(\begin{array}{l}\left(\begin{array}{l}-(\kappa_0-\sqrt{\kappa_0^2-\delta})v_0X_0^2+(\kappa_0-\sqrt{\kappa_0^2-\delta})\\(-\kappa_0+\kappa_0v_0c_{220}-v_0+v_0^2c_{220}-v_0c_{220}\sqrt{\kappa_0^2-\delta}-\sqrt{\kappa_0^2-\delta})X_0+\\(\kappa_0-\sqrt{\kappa_0^2-\delta})(\kappa_0+v_0+\sqrt{\kappa_0^2-\delta})c_{220}(\kappa_0+v_0-\sqrt{\kappa_0^2-\delta})\end{array}\right)\\\sqrt{\kappa_0+\sqrt{\kappa_0^2-\delta}}+\\\left(\begin{array}{l}(\kappa_0+\sqrt{\kappa_0^2-\delta})v_0X_0^2-(\kappa_0+\sqrt{\kappa_0^2-\delta})\left(\begin{array}{l}-\kappa_0+\kappa_0v_0c_{220}-v_0+v_0^2c_{220}+\\v_0c_{220}\sqrt{\kappa_0^2-\delta}+\sqrt{\kappa_0^2-\delta}\end{array}\right)X_0\\-(\kappa_0+\sqrt{\kappa_0^2-\delta})(\kappa_0+v_0-\sqrt{\kappa_0^2-\delta})c_{220}(\kappa_0+v_0+\sqrt{\kappa_0^2-\delta})\end{array}\right)\\\sqrt{\kappa_0-\sqrt{\kappa_0^2-\delta}}\end{array}\right)\Bigg/\left(2\sqrt{\kappa_0^2-\delta}\sqrt{\kappa_0-\sqrt{\kappa_0^2-\delta}}(1+X_0)\sqrt{\kappa_0+\sqrt{\kappa_0^2-\delta}}(v_0c_{220}+1)\right), \tag{A.21}$$

$$d_0 = \left(\begin{array}{l}\left(\begin{array}{l}-c_{220}(\kappa_0^2-\delta)+X_0(v_0c_{220}+1)\sqrt{\kappa_0^2-\delta}+(\kappa_0+v_0X_0+v_0)\\(c_{220}\kappa_0+v_0c_{220}-X_0)\end{array}\right)\\\sqrt{\kappa_0+\sqrt{\kappa_0^2-\delta}}+\left(\begin{array}{l}c_{220}(\kappa_0^2-\delta)+X_0(v_0c_{220}+1)\sqrt{\kappa_0^2-\delta}\\-(\kappa_0+v_0X_0+v_0)(c_{220}\kappa_0+v_0c_{220}-X_0)\end{array}\right)\sqrt{\kappa_0-\sqrt{\kappa_0^2-\delta}}\end{array}\right)\Bigg/\left(2\sqrt{\kappa_0+\sqrt{\kappa_0^2-\delta}}\sqrt{\kappa_0-\sqrt{\kappa_0^2-\delta}}\sqrt{\kappa_0^2-\delta}(v_0c_{220}+1)\right). \tag{A.22}$$

References

ANSYS General Purpose Finite Element Program, Release 11 Documentation for ANSYS, 2007.

Bao, G., Cai, H., 1997. Delamination cracking in functionally graded coating/metal substrate systems. Acta Materialia 45, 1055–1066.

Bazant, Z.P., Cedolin, L., 2003. Stability of Structures: Elastic, Inelastic, Fracture and Damage Theories. Dover Publications, Inc.

Chen, J., Liu, Z.X., Zou, Z.Z., 2002. Transient internal crack problem for a nonhomogeneous orthotropic strip (Mode I). International Journal of Engineering Science 40, 1761–1774.

Chen, J., 2005. Determination of thermal stress intensity factors for an interface crack in a graded orthotropic coating-substrate structure. International Journal of Fracture 133, 303–328.

Chiu, T.C., Erdogan, F., 2003. Debonding of graded coatings under in-plane compression. International Journal of Solids and Structures 40, 7155–7179.

Dag, S., Yildirim, B., Erdogan, F., 2004. Interface crack problems in graded orthotropic media: analytical and computational approaches. International Journal of Fracture 130, 471–496.

Dag, S., 2006. Thermal fracture analysis of orthotropic functionally graded materials using an equivalent domain integral approach. Engineering Fracture Mechanics 73, 2802–2828.

Dag, S., Yildirim, B., Sarikaya, D., 2007. Mixed-mode fracture analysis of orthotropic functionally graded materials under mechanical and thermal loads. International Journal of Solids and Structures 44, 7816–7840.

Delale, F., Erdogan, F., 1983. The crack problem for a nonhomogeneous plane. ASME Journal of Applied Mechanics 50, 609–614.

El-Borgi, S., Erdogan, F., Ben Hatira, W., 2003. Stress intensity factors for an interface crack between a functionally graded coating and a homogeneous substrate. International Journal of Fracture 123, 139–162.

El-Borgi, S., Keer, L., Ben Said, W., 2004. An embedded crack in a functionally graded coating bonded to a homogeneous substrate under frictional hertzian contact. Wear, An International Journal on the Science and Technology of Friction, Lubrication and Wear 257, 760–776.

El-Borgi, S., Hidri, L., Abdelmoula, R., 2006a. An embedded crack in a graded coating bonded to a homogeneous substrate under thermo-mechanical loading. Journal of Thermal Stress 29, 439–466.

El-Borgi, S., Aloulou, W., Zghal, A., 2006b. Buckling of a functionally graded coating with an embedded crack bonded to a homogeneous substrate. International Journal of Fracture 142, 137–150.

Erdogan, F., Gupta, G.D., Cook, T.S., 1973. Numerical solution of singular integral equations. In: Sih, G.C. (Ed.), Mechanics of Fracture. Norrdhoff, Leyden, pp. 368–425.

Erdogan, F., 1995. Fracture mechanics of functionally graded materials. Composites Engineering 5, 753–770.

Erdogan, F., Wu, B.H., 1996. Crack problems in FGM layers under thermal stresses. Journal of Thermal Stresses 19, 237–265.

Feng, W.J., Zhang, Z.G., Zou, Z.Z., 2003. Impact failure prediction of mode III crack in orthotropic functionally graded strip. Theoretical and Applied Fracture Mechanics 40, 97–104.

Grimes, R.G., Lewis, J.G., Simon, H.D., 1994. A shifted block Lanczos algorithm for solving sparse symmetric generalized eigenproblems. SIAM Journal Matrix Analysis Applications 15 (1), 228–272.

Gu, P., Asaro, R.J., 1997. Cracks in functionally graded materials. International Journal of Solids and Structures 34, 1–17.

Guo, L.-C., Wu, L.-Z., Zeng, T., Ma, L., 2004. Mode I crack problem for a functionally graded orthotropic strip. European Journal of Mechanics A/Solids 23, 219–234.

Guo, L.-C., Wu, L.-Z., Zeng, T., 2005. The dynamic response of an edge crack in a functionally graded orthotropic strip. Mechanics Research Communications 32, 385–400.

Holt, J., Koizumi, M., Hirai, T., Munir, Z.A. (Eds.), 1992. Functionally Gradient Materials. Ceramic Transactions, vol. 34. The American Ceramic Society, Ohio.

Kaysser, W.A., Ilschner, B., 1995. FGM research activities in Europe. MRS Bulletin 20, 22–26.

Kim, J.-H., Paulino, G.H., 2002. Mixed-mode fracture of orthotropic functionally graded materials using finite elements and the modified crack closure method. Engineering Fracture Mechanics 69, 1557–1586.

Kim, J.-H., Paulino, G.H., 2003a. Mixed-mode J-integral formulation and implementation using graded elements for fracture analysis of nonhomogeneous orthotropic materials. Mechanics of Materials 35, 107–128.

Kim, J.-H., Paulino, G.H., 2003b. The interaction integral for fracture of orthotropic functionally graded materials: evaluation of stress intensity factors. International Journal of Solids and Structures 40, 3967–4001.

Kurihara, K., Sasaki, K., Kawarada, M., 1990. Adhesion improvement of diamond films. In: Yamanouchi, M., Koizomi, M., Hirai, T., Shiota, I. (Eds.), FGM'90, Proceedings of the 1st International Symposium on Functionally Gradient Materials, FGM Forum, Tokyo, Japan, pp. 65–69.

Lanhe, W., 2004. Thermal buckling of a simply supported moderately thick rectangular FGM plate. Composite Structures 64, 211–218.

Lee, Y.-D., Erdogan, F., 1995. Residual/thermal stresses in FGM and laminated thermal barrier coatings. International Journal of Fracture 69, 145–165.

Liew, K.M., Yang, J., Kitipornchai, S., 2003. Post-buckling of piezoelectric FGM plates subject to thermo-electro-mechanical loading. International Journal of Solids and Structures 40, 3869–3892.

Ma, L.S., Wang, T.J., 2003. Nonlinear bending and post-buckling of a functionally graded circular plate under mechanical and thermal loadings. International Journal of Solids and Structures 40, 3311–3330.

Ma, L.S., Wang, T.J., 2004. Relationships between axisymmetric bending and buckling solutions of FGM circular plates based on third-order plate theory and classical plate theory. International Journal of Solids and Structures 41, 85–101.

Ozturk, M., Erdogan, F., 1997. Mode I crack problem in an inhomogeneous orthotropic medium. International Journal of Engineering Science 35, 869–883.

Ozturk, M., Erdogan, F., 1999. The mixed mode crack problem in an inhomogeneous orthotropic medium. International Journal of Fracture 98, 243–261.

Pindera, M.J., Aboudi, J., Arnold, S.M., 2002. Analysis of spallation mechanism in thermal barrier coatings with graded bond coats using the higher-order theory for FGMs. Engineering Fracture Mechanics 69, 1587–1606.

Rajakumar, C., Rogers, C.R., 1991. The Lanczos algorithm applied to unsymmetric generalized eigenvalue problems. International Journal for Numerical Method in Engineering 32, 1009–1026.

Rao, B.N., Rahman, S., 2005. A continuum shape sensitivity method for fracture analysis of orthotropic functionally graded materials. Mechanics of Materials 37, 1007–1025.

Shen, H.S., 2003. Post-buckling analysis of pressure-loaded functionally graded cylindrical shells in thermal environments. Engineering Structures 25, 487–497.

Sampath, S., Herman, H., Shimoda, N., Saito, T., 1995. Thermal spray processing of FGMs. MRS Bulletin 20 (1), 27–31.